

NUMERICAL ANALYSIS OF VHCF CRUCIFORM TEST SPECIMENS WITH NON-UNITARY BIAXIALLITY RATIOS

DIOGO MONTALVÃO^{1,*}, ATTILA BLASKOVICS¹, PEDRO COSTA², LUÍS REIS² & MANUEL FREITAS²

¹ Department of Design and Engineering, Faculty of Science and Technology, Bournemouth University, United Kingdom.

² Department of Mechanical Engineering, Instituto Superior Técnico, University of Lisbon, Portugal.

ABSTRACT

With the development of new materials, it is now known that there is no such thing as a fatigue endurance limit, i.e. materials do not have infinite life when the stress level is such that there is no fracture up to 10 million (1E7) cycles. The problem of testing materials above this number of cycles is that most testing equipment operates well below 150 Hz, making testing up to 1 billion (1E9) cycles or above is an impracticality. The recent developments of ultrasonic testing machines where frequencies can go as high as 20 kHz or above enabled tests to be extended to these ranges in just a few days. This is known as very high cycle fatigue (VHCF). On the other hand, critical components used in engineering applications are usually subjected to multi-axial loads, as is the case of the fuselage and wings of aircrafts which are subjected to biaxial states of stress. In this paper, VHCF cruciform test specimens purposely designed to develop orthogonal biaxial stresses with different biaxiality ratios will be analysed. The specimens are composed from Aluminium 6082-T651, a medium strength alloy used in many highly stressed engineering applications, including trusses, cranes, bridges and transportation. The specimens work as tuning forks with determined mode shapes at 20 ± 0.5 kHz, where maximum principal stresses are developed at the centre of the specimen. Finite element analysis (FEA) is used to assess the dynamic behaviour of the specimens. The framework on how to design and manufacture cruciform specimens with different biaxiality ratios will be explained in a clear way so it can be used by other engineers in the field.

Keywords: Biaxial Stresses; Cruciform Specimens; Very High Cycle Fatigue; Ultrasonic Testing.

1 INTRODUCTION

According to some authors, 90% of all metallic failures are estimated to be due to fatigue [1]. The emergence of new technologies and manufacturing processes, together with the need to increase the lifetime and safety of mechanical systems, led to the need to increase the fatigue life of mechanical components [2]. Thus, the high quality standards of industries dealing with cyclic-load bearing components demand predictability and updated fatigue data to design mechanical components that will be subjected to extended lifetimes in comparison to the past [3]. However, fatigue properties, especially in the very high cycle fatigue (VHCF) regimen up to 1E9 cycles, have not been sufficiently determined yet [4].

With the development of other new materials, such as high strength aluminium alloys with a different microstructure from steels, materials no longer have ‘infinite life’ in the classical sense, where it was accepted that the fatigue limit is the stress level such that there is no fracture up to 1E7 cycles [3, 5, 6]. This led to conclude the need to improve the S–N (stress vs cycles to failure) diagrams and eliminate the endurance limit [5, 7].

New testing equipment, such as ultrasonic testing machines, allowed for the extension of the concept of fatigue up to 1E9 cycles and even more [8, 9]. This area of studies is now known as gigacycle or VHCF. With an ultrasonic machine operating at 20 kHz the length of time required to reach 1E9 cycles could be reduced, in theory, to as little as 14 h, if no

* ORCID: <https://orcid.org/0000-0003-1108-0475>

interruptions had to be made. With conventional testing machines operating in the 20 Hz to 150 Hz range the same test would take between 3 months to over 1 year.

On the other hand, most of the existing test equipment in the market for both classical and VHCF are uniaxial test machines [10], in the sense that the state of stress created is unidirectional. However, critical components used by the aerospace, automotive, energy, naval, medical, space, and other industries are usually subjected to complex multi-axial loading conditions [11, 12]. Typical biaxial in-plane fatigue machines require that the centre of the specimen does not move during the test, meaning that the actuators (usually four) must be precisely synchronised [10, 13]. Furthermore, the almost only available in-plane biaxial machines so far in the market use are the servo-hydraulic actuators. Thus, these machines are not good candidates to be used in VHCF.

In a few recent papers [14, 15], an original approach to biaxial fatigue testing in the VHCF regimen (Fig. 1), was proposed. Having the same principles used in the design of the VHCF machines as in [3, 8, 16], it was shown that, at least when using cruciform specimens for in-plane axial–axial (biaxial) testing, only the specimen needs to be redesigned. No changes

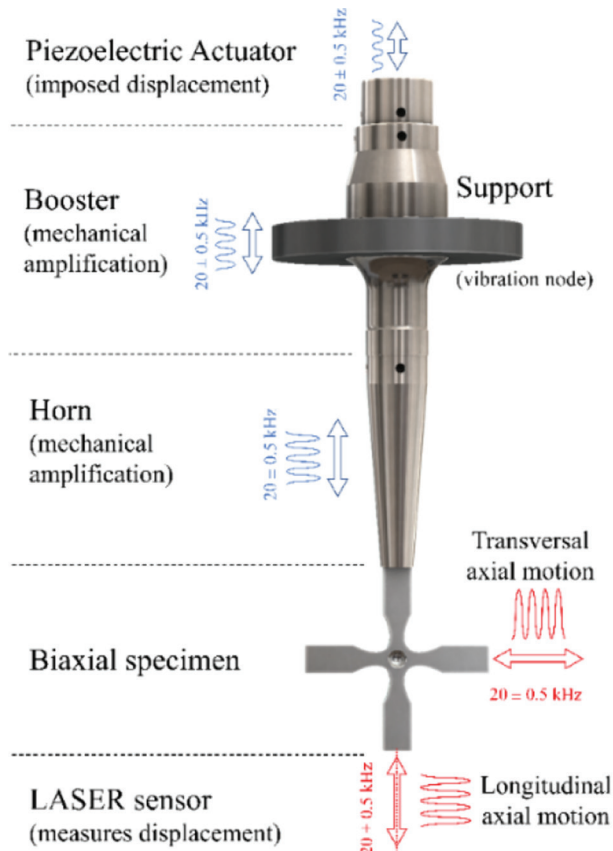


Figure 1: VHCF testing machine resonant system components with biaxial specimen being tested.

Source: (Montalvão and Wren, 2017).

are required to be made to the machine. For example, in a work where combined axial-torsion is obtained, the horn had to be redesigned [9]. The redesign of existing specimens can be achieved by the application of a dimensional scale factor, which is inversely proportional to the natural frequencies [14], but there are other possibilities as will be presented in this paper. Therefore, and in principle, any existing specimen that is already designed for in-plane axial–axial (biaxial) fatigue testing, such as typical cruciform specimens, could be scaled down (or up) so that their natural frequencies are adjusted to meet the requirements of VHCF ultrasonic test machines like the ones mentioned above.

This paper is an extension to the Montalvão *et al.*'s [17] presentation, where existing cruciform test specimens are re-designed so that they can be used to create an in-plane biaxial state of stress in 'uniaxial' VHCF ultrasonic testing machines. It is also shown how to get different biaxiality stress ratios. The framework on how to design these specimens is laid out in a clear way through the presentation of the design principles, so that other researchers in the field can engage in the exciting range of opportunities that are now opened with the outcomes from this research work.

2 DESIGN PRINCIPLES OF CRUCIFORM SPECIMENS FOR VHCF

In the system shown in Fig. 1, a piezoelectric actuator introduces a pure axial harmonic vibration at 20 ± 0.5 kHz (this system is based on the existing one at Instituto Superior Técnico in the University of Lisbon in Portugal [2, 3, 8, 14, 15]). This vibration is transmitted and amplified through a system composed by a booster (where the whole assembly is supported) and a horn, down to the specimen. These four parts form the resonant system of the testing machine. The principle of operation of the vibration system is based on free vibration resulting in a minimum of contact force between the elements in the system. Each element in the resonant system is manufactured to have the same axial fundamental frequency and vibrate in phase opposition at the contact points. Therefore, one important aspect to take into consideration is that the test specimen must be designed to have a certain mode shape tuned to the operating frequency of the machine, in this case 20 ± 0.5 kHz (19.5–20.5 kHz).

2.1 Tuning through the application of a global dimensional scale factor

Existing cruciform specimens, such as the ones proposed in [13], can be tuned so that the resonant frequency of a given mode shape is the same as the machine's operating frequency, simply through the application of an enlargement or reduction in the geometrical scale factor [14]:

$$s = \frac{f_{UD}}{f_{CD}} \quad (1)$$

where f_{UD} is the frequency of that particular mode shape in the original (or uncalibrated) design and f_{CD} is the new frequency of that particular mode shape in the new (or calibrated) design. In the case of an ultrasonic testing machine operating at 20 ± 0.5 kHz, $f_{CD} = 20$ kHz.

The mode shapes that are being sought are axial mode shapes (i.e. where the cruciform specimens' arms extend or compress during vibration). There are two possible axial mode shapes [14], although only one is at 20 kHz at any one time (Fig. 2). Mode C-T corresponds to a situation where the axes are out-of-phase, i.e. when one of the axes is under tension the other axis is under compression. In this case, the in-plane stresses are fully reversed and the biaxiality ratio is $B = -1$, since it is defined as

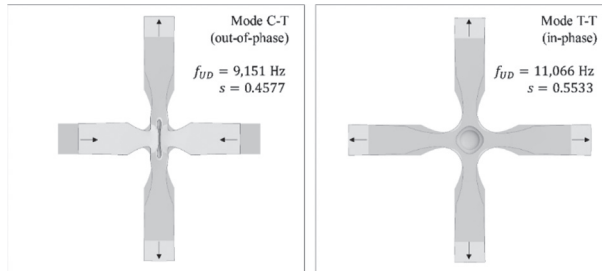


Figure 2: Cruciform test specimens' first two axial mode shapes (deformation is exaggerated for better understanding): C-T (compression–tension) (out-of-phase) and T-T (tension–tension) (in-phase).

Source: (Montalvão and Wren, 2017.)

$$B = \frac{\sigma_y}{\sigma_x} \quad (2)$$

where σ_x is the stress in the x (or horizontal)-direction and σ_y is the stress in the y (or vertical)-direction. Mode T-T corresponds to a situation where both axes are in-phase, i.e. they are both either under tension or under compression simultaneously. In this case, the biaxiality ratio is $B = 1$.

The strain ε at the centre of the uniaxial specimen can be determined from the measurement of the displacement u of the specimen's tip [8]. The stress is then determined through the application of Hooke's law, i.e. $\sigma = E\varepsilon$, where E is the Young's modulus of the material. Therefore, it is reasonable to assume that the biaxiality ratio can also be determined from

$$B = \frac{u_y}{u_x} \quad (3)$$

where u_x and u_y are the displacements in the horizontal and vertical directions, respectively. This approximation is true as long as most of the deformation happens at the central section of the specimen, i.e. at the rectangular ends of the specimen motion is mostly rigid body motion in comparison.

Because these specimens are symmetric and only one actuator is used, both C-T and T-T specimens are designed to be tested under fully reversed cyclic loading in both directions, as in other VHCF test methods [8], i.e.:

$$R = \frac{\sigma_{x,min}}{\sigma_{x,max}} = \frac{\sigma_{y,min}}{\sigma_{y,max}} = -1. \quad (4)$$

2.2 Tuning through changing the lengths of the specimen arms

The problem with the simple application of a scale factor is that the scale factor changes the whole geometry of the specimen, including the central section (Fig. 3), where the stresses achieve their maximum values [13].

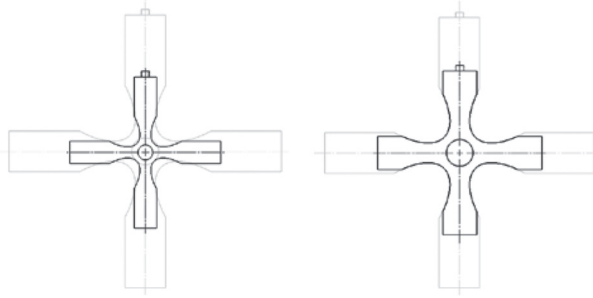


Figure 3: Result from the ‘scaling’ (left) and from the ‘change in arms’ lengths’ (right) methods to achieve a design that delivers an in-phase (T-T) mode shape at 20 kHz.

This may not be desirable due to practicality and modelling issues or when comparing specimens that are intended to have biaxiality ratios different from one, as the specimens would all have different central sections. In order to overcome this, an alternative method is suggested whereby the rectangular ends of the arms have their lengths changed [17].

If one considers the approximation that one single arm of the cruciform specimen behaves as a rod with a lump mass at the tip under free longitudinal vibration, then the increase in mass at the tip will lead to a reduction in the natural frequency f_n , and vice versa, as illustrated by the following equation:

$$f_n = \frac{1}{2\pi} \sqrt{\frac{AE}{mL}} \quad (5)$$

where A is the cross-sectional area of the idealised rod, L is its length, E is the Young’s modulus of the rod’s material, and m is value of the lump mass at the tip.

However, these cruciform specimens are not composed of uniform rods with lump masses at their tips, so although the basic idea can be explored, equation (5) cannot be formally used. Instead, using FEA, this approximation was proposed to be used to tune the original specimens from [13] so that the required C-T and T-T mode shapes at 20 kHz were obtained without affecting the geometry of the specimens’ central area [17]. The result was a cruciform specimen with the same central section geometry and thickness as the original specimen, but only slightly shorter (or even narrower) arms’ (Fig. 3).

2.3 Obtaining specimens with non-unitary biaxiality ratios

The same principles as the ones described in the previous section, namely the one that is based on the ‘change in arms’ lengths’ (Section 2.2), can also be used to design specimens that are able to deliver biaxiality ratios $B \neq \pm 1$ ($B > 0 \wedge B \neq 1$ for specimen T-T; and $B < 0 \wedge B \neq -1$ for specimen C-T).

When biaxiality ratios $B \neq \pm 1$ are being sought, this can be achieved by changing the arms’ lengths in different directions by different proportions. For example, let us assume that the starting point is the calibrated design from Fig. 3 on the right. If the arm in the horizontal direction is slightly shortened by a quantity $-\Delta x$, and using again the analogy of a rod with a lump mass at the tip, this corresponds to a reduction in the mass in the horizontal direction;

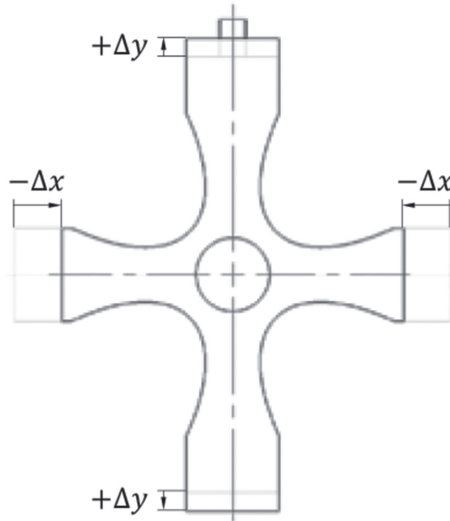


Figure 4: Result from the ‘change in arms’ lengths’ method (black model) to obtain an out-of-phase C-T specimen with a non-unitary biaxiality ratio at 20 kHz.

hence, to an increase in the natural frequency according to eqn (2). To compensate for this increase in the natural frequency, the arm in the vertical direction has to be slightly extended by a quantity $+\Delta y$ until the frequency is reduced back to 20 kHz. Since the elongation of one arm corresponds to an increase in mass, eqn (5) tells us that the frequency can be reduced this way. Fig. 4 shows one example of how a specimen with a non-unitary biaxiality ratio may look like following the aforementioned procedure.

Unfortunately, the complexity of the geometry of the cruciform specimens is such that it is not easy to derive analytical solutions for both mode shapes. Therefore, FEA is used instead. Once a few models have been obtained (through, for example, trial-and-error), it will be possible to determine a trend and derive an equation that will allow getting the necessary parameters to obtain other biaxiality ratios, as is shown in section 3 with a few examples.

3 NUMERICAL MODELS AND RESULTS

The results presented herewith are based on numerical FEA models that are part of on-going work whose details are in [18]. The specimens from [13] were re-designed so that non-unitary biaxiality ratios could be obtained. In this approach, the design process was the following:

- Determination of the dimensions of base specimens (with $|B| = \pm 1$), following a combination of the procedures described in Sections 2.1 and 2.2;
- Determination of the new dimensions from the base specimens so that $|B| \neq \pm 1$, following the procedure described in Section 2.3;
- The specimens were initially designed under free-free boundary conditions, since the nature of operation of ultrasonic fatigue testing machines is that they seek to reproduce free vibration with the specimen vibrating at its own natural frequency. In other words, the connection between specimen and horn (Fig. 1) is made through vibration anti-nodes and should have little influence on modes C-T and T-T (however, other modes may be influenced, as briefly discussed in Section 3.1).

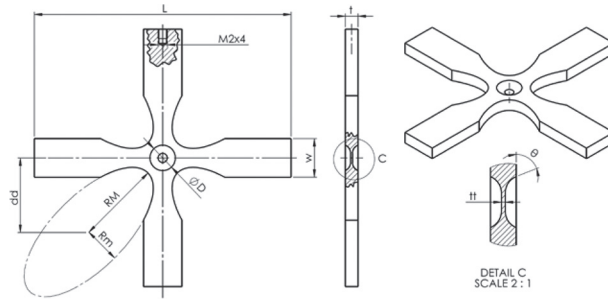


Figure 5: Cruciform test specimen's dimensions [14].

The material chosen was Aluminium 6082-T651, a medium strength alloy used in many highly stressed engineering applications, including trusses, cranes, bridges and transportation.

3.1 Dimensions of the base specimens ($|B| = \pm 1$)

The basic procedure for the determination of the dimensions (Fig. 5) of the base specimens has briefly been described in Sections 2.1 and 2.2 (the scaling method described in Section 2.1 is used to control the thickness of the specimen only). However, what this does not show is that there may be problems related to the existence of other mode shapes in the vicinity of the mode shapes of interest. In such a case, those modes will have an influence on the mechanical behaviour of the specimens, as [18] demonstrated by both numerical and experimental results. There is a bending mode shape that resembles the ‘flapping’ of a bird in the vicinity of the axial mode shapes C-T and T-T (i.e. with a resonant frequency close to 20 kHz). This may interfere with the intended specimens’ behaviour. Therefore, a quick analysis was done so that these ‘flapping’ mode shapes would be sufficiently far away from the operating frequency range of interest (19.5 to 20.5 kHz).

The starting point was the optimised 10 mm thickness specimen from [13]. Since this is the thickest specimen presented in [13], and it is known from Modal Analysis (and most textbooks will say it, e.g. [19]) that the thicker a beam is the higher the frequencies of its mode shapes (i.e. there will be less mode shapes in any frequency range starting from 0 Hz), this design was the best candidate to be adjusted following the method described in Section 2.2. Results for the ‘flapping’ mode shapes’ frequencies obtained for a few of the designs tested are shown in

Table 1: Assessment of the influence of the “flapping” mode shape on different models (taking as starting point the 10 mm specimen from Baptista et al., 2014).

Specimen Type	New thickness (mm)	'Flapping' mode freq. (Hz)	Diff. to 20 kHz freq. (%)
TT	6	20018	0.09
CT	6	22084	10.4
TT	8	20530	2.65
CT	8	21347	6.74
TT	10	21074	5.37
CT	10	22358	11.79

Table 1 (this time, the simulations considered the assembly of the specimen in the machine, since the connecting point between horn and specimen is not at an anti-node of the flapping mode shape, as shown in [18]). It can be seen that both the T-T and C-T specimens with 8 and 10 mm thicknesses have the ‘flapping’ mode shapes’ frequencies outside the ultrasonic fatigue testing machine’s operational frequency of 19.5–20.5 kHz and more than 2.6% away from the 20 kHz, which means they should not be of great concern. In the current paper, the 8 mm thickness was chosen, since this should allow for higher stresses to be obtained in the central section for a lower power setting of the ultrasonic fatigue testing machine than for a 10 mm thickness specimen. The final dimensions of the resulting base specimens can be found in Table 2.

3.2 Dimensions of non-unitary biaxiality ratio specimens ($|B| \neq \pm 1$)

In this paper, the only dimensional differences from non-unitary biaxiality ratio specimens ($|B| \neq \pm 1$) to unitary ones ($|B| = \pm 1$), is that the length in the x (horizontal) and y (vertical)-directions are different in the same specimen, i.e.:

$$\begin{aligned} L_x &= L \pm \Delta_x \\ L_y &= L \mp \Delta_y \end{aligned} \quad (6)$$

where L is the length from table 2, Δ_x is the change in length in the x direction, and Δ_y is the change in length in the y direction. It is important to note that, although the absolute values of Δ_x and Δ_y are expected to be different from one another, if one is positive the other has to be negative, so that the mode shape’s resonant frequency does not shift away from 20 kHz (i.e. one serves to ‘balance’ the frequency change introduced by the other). Table 3 and Fig. 6 show some dimensional change combinations Δ_x vs Δ_y so that the resulting mode shape resonant frequency is as close as possible to 20,000 Hz. Note that Table 3 presents both the biaxiality ratio as defined by eqn (2) as well as its inverse.

These results allow for the following observations to be made:

- The specimens are producing non-unitary biaxiality ratios that increase with the change in arms’ lengths, as predicted. In fact, the absolute value of the biaxiality ratio is very close to the absolute value of the inverse of the ratio between the corresponding dimensional changes in both directions, i.e. $|B| = \left| \frac{u_y}{u_x} \right| \cong \left| \frac{\Delta_x}{\Delta_y} \right|$. The main reason why they are not exactly the same is related to the fact that the rectangular tips of the specimens are not lump rigid masses and also deform elastically, although this is much less relevant than at the specimen’s centre;
- Fig. 6 shows that the data follow trendlines with R-squared coefficients of correlation close to 1. This means that, unless there are any practical issues, these equations can be

Table 2: Dimensions of the base specimens ($|B| = \pm 1$) using the notation from Fig. 5.

	L (mm)	w (mm)	t (mm)	RM (mm)	Rm (mm)	dd (mm)	D (mm)	tt (mm)	θ (°)
CT	93.52	20	8	52.16	22.85	46.14	15.83	1.2	70.34
TT	119.0	20	8	52.16	22.85	46.14	15.83	1.2	70.34

Table 3: Changes in arms' lengths and biaxiality ratios for $|B| \neq \pm 1$ specimens.

Model	Specimen type C-T				Specimen type T-T				
	Δy (mm)	Δx (mm)	B	B^{-1}	Model	Δy (mm)	Δx (mm)	B	B^{-1}
CT 1	1.5	-1.95	-1.30	-0.77	TT 1	1.5	-1.2	0.82	1.23
CT 2	2	-2.85	-1.44	-0.70	TT 2	2	-1.55	0.77	1.31
CT 3	2.5	-4.05	-1.62	-0.62	TT 3	3	-2.05	0.69	1.45
CT 4	3	-5.5	-1.84	-0.54	TT 4	4	-2.5	0.62	1.61
CT 5	3.25	-6.4	-1.97	-0.51	TT 5	10	-4	0.40	2.49
CT 6	3.75	-8.65	-2.31	-0.43	TT 6	17.5	-4.85	0.28	3.52
CT 7	4	-10.1	-2.52	-0.40	TT 7	27.5	-5.45	0.21	4.70

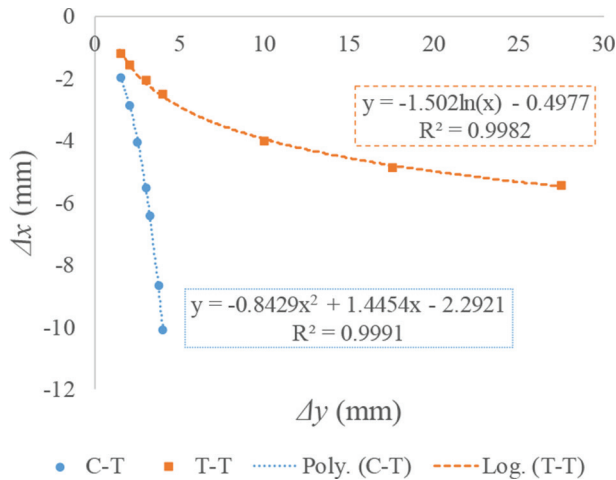


Figure 6: Plot of the change in arm's length in the x -direction Δ_x with the change in arm's length in the y -direction Δ_y for $|B| \neq \pm 1$ specimens.

used to estimate (at least arithmetically) any other combinations of Δ_x vs Δ_y for a set 20,000 Hz resonant frequency of the given mode shape.

- There are some limitations in the maximum biaxiality ratio that can be obtained. This is more visible for specimen C-T from model CT7 with a biaxiality ratio $B = 2.52$, where $\Delta_x = -10.1$ mm. This limitation is related to the lengths of the cruciform specimen's arms which are shorter in the case of the out-of-phase C-T specimen: 12.1 mm long (each) against about twice as much for specimen T-T.
- If we compare the biaxiality ratios B of C-T out-of-phase specimens with the inverse of the biaxiality ratios B^{-1} of T-T in-phase specimens (and *vice versa*) we observe that their absolute values are closely related. As an example, let us compare model CT1 with model TT2. The following can be observed:

- o The biaxiality ratio of model CT1 has approximately the same absolute value as the inverse of the biaxiality ratio of model TT2, i.e. $-B_{CT1} \cong B_{TT2}^{-1} \cong 1.3$;
- o The changes in arms lengths in both directions for models CT1 and TT2 seem to be swapped in terms of value and signal, i.e. $\Delta_{yCT1} \cong -\Delta_{xTT2} \wedge \Delta_{xCT1} \cong -\Delta_{yTT2}$;
- The previous point shows how ‘closely related’ modes C-T and T-T are, as the same observations apply to other of the studied models, e.g.:
 - o $-B_{CT2} \cong B_{TT3}^{-1} \cong 1.4$ and $\Delta_{yCT2} \cong -\Delta_{xTT3} \wedge \Delta_{xCT2} \cong -\Delta_{yTT3}$;
 - o $-B_{CT3} \cong B_{TT4}^{-1} \cong 1.6$ and $\Delta_{yCT3} \cong -\Delta_{xTT4} \wedge \Delta_{xCT3} \cong -\Delta_{yTT4}$;
 - o $-B_{CT7} \cong B_{TT5}^{-1} \cong 2.5$ and $\Delta_{yCT7} \cong -\Delta_{xTT5} \wedge \Delta_{xCT7} \cong -\Delta_{yTT5}$.
- Based on the observations above, if we now plot Fig. 6, but rotating the axes 90° for one of the specimens only, e.g. T-T, and plotting their absolute values, Fig. 7 is obtained. It can be seen that there is an ‘almost perfect’ correlation between the changes in arms lengths for both specimens’ types C-T and T-T.

3.3 Re-defining the biaxiality ratio for in-plane cruciform specimens

The final results to be discussed in this paper are a plot of the biaxiality ratio B and a plot of the inverse of the biaxiality ratio B^{-1} with respect to the change in arms’ lengths in the x - and y -directions, respectively (Fig. 8).

First of all, it can be seen that these relationships are linear and that all plots have similar slopes (consistent with the previous observation that specimens C-T and T-T are correlated). The intersection at the origins are at either $B = 1$ (for specimen T-T) or $B = -1$ (for specimen C-T). These two correspond to situations where the specimens are symmetric, hence with unitary biaxiality ratios.

Secondly, it is possible to see that there are ‘limits’ to the biaxiality ratios:

- If one looks to the biaxiality ratio (B) plot for specimen T-T in Fig. 8, the biaxiality ratio becomes zero for $\Delta x = -6.811$ mm. From equations (2) and (3) this is equivalent to a situation where stress is uniaxial in the x -direction of specimen T-T (perpendicular to the

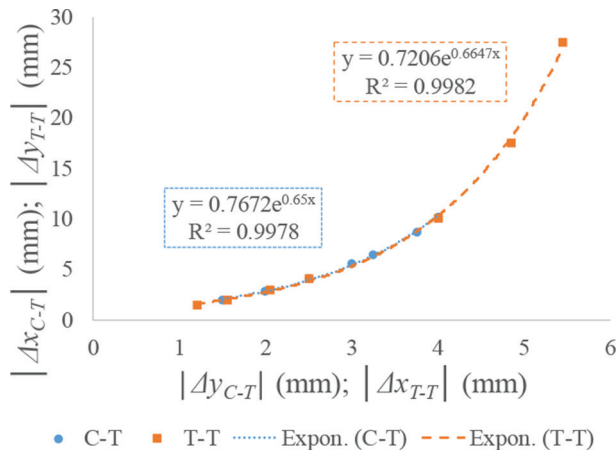


Figure 7: Re-plot of Fig. 6 where the absolute values of the axes are used and the axes were rotated 90° for specimen T-T, highlighting the ‘overlap’ between data.

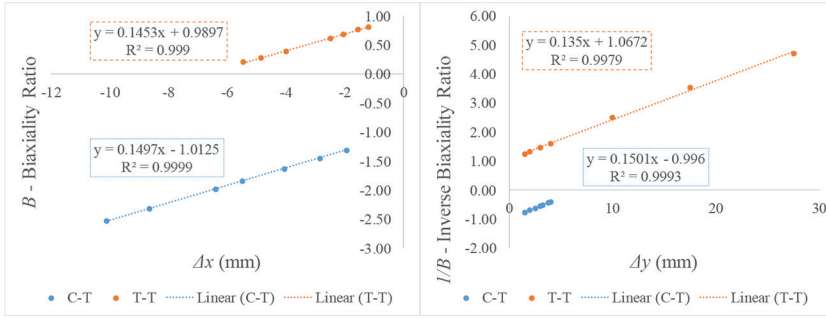


Figure 8: Plots of the biaxiality ratio B (left) and the inverse of the biaxiality ratio B^{-1} (right) with respect to the change in arm’s length in one direction.

horn in Fig. 1), with no motion (or stress) in the y -direction;

- If one now looks to the inverse of the biaxiality ratio (B^{-1}) plot for specimen C-T, this becomes zero when $\Delta y = +6.636$ mm. This would be equivalent to having specimen C-T with a uniaxial stress in the y -direction, with no deformation (or stress) in the x direction;
- If the biaxiality ratio for specimen T-T is $B = 0$ when $\Delta x = -6.811$ mm, then $B^{-1} \rightarrow +\infty$ and $\Delta y \rightarrow +\infty$, which is an impracticality;
- If the inverse of the biaxiality ratio for specimen C-T is $B^{-1} = 0$ when $\Delta y = +6.636$ mm, then $B \rightarrow -\infty$ and $\Delta x \rightarrow -\infty$, which is another impracticality.

These last results are particularly important for the definition of the biaxiality ratio in cruciform test specimens for VHCF, because it is easier to work with limited intervals rather than with intervals that can range up to infinite. It is therefore proposed that the biaxiality ratio as initially defined in equation (2) is formally defined as

$$B = \begin{cases} \sigma_y / \sigma_x \text{ if } |\sigma_x| \geq |\sigma_y| \\ \sigma_x / \sigma_y \text{ if } |\sigma_x| < |\sigma_y| \end{cases} \quad (7)$$

so that $B \in [-1, 1]$. The inverse of the biaxiality ratio would hence be defined in the interval $]-\infty, -1] \cup [1, +\infty[$. By defining the biaxiality ratio as in eqn (7), this means that for $B = \pm 1$ we have the same in-plane stresses in both directions and for the limit case where $B = 0$ we have uniaxial stress in one direction only. The other advantage of eqn (7) is that, as a matter of convenience, the biaxiality ratio could also be expressed as a percentage, where the signal is indicating if the mode shape is either in-phase (+) or out-of-phase (-).

4 CONCLUSION

The current paper discussed non-unitary biaxiality ratio cruciform specimens that can be used in ultrasonic VHCF machines. It is shown, by numerical results, that this is possible to achieve by ‘tuning’ existing designs of in-plane cruciform specimens using simple principles, such as the application of a global dimensional scale factor and/or controlled changes in the arms’ lengths. Two types of designs were discussed: C-T, where the biaxiality ratio is negative since the arms deformation is out-of-phase, and T-T where the biaxiality ratio is positive since the arms deformation is in-phase. One important result from the analysis is that, in

order to make the comparison between different specimens consistent, the biaxiality ratio was proposed to be defined in such a way that it becomes a limited function between -1 and 1 . Within this definition, for $B = \pm 1$ the same values of in-plane stresses are generated in both directions, and for $B = 0$ the specimen is under uniaxial stress. This avoids having a situation where the biaxiality ratio, if defined by its inverse, may tend to infinity, which can be impractical.

The next steps of this research are to actually produce the test specimens, calibrate them (i.e. find correlations between the displacements at the tips and the stresses developing at the centre) and test them in an ultrasonic VHCF testing machine.

REFERENCES

- [1] Suryanarayana, C., *Experimental Techniques in Materials and Mechanics*, CRC Press: Boca Raton, 2011.
- [2] Anes, V., Montalvão, D., Ribeiro, A., Freitas, M. & Fonte, M., Design and instrumentation of an ultrasonic fatigue testing machine. *Proceedings of the 5th International Conference on Very High Cycle Fatigue*, Berlin, Germany, 2011.
- [3] Freitas, M., Anes, V., Montalvão, D., Reis, L. & Ribeiro, A., Design and assembly of an ultrasonic fatigue testing machine. *Proceedings of the 28th Encuentro del Grupo Español de Fractura (Anales de Mecánica de la Fractura)*, Gijón, Spain, 2011.
- [4] Wycisk, E., Siddique, S., Herzog, D., Walther, F. & Emmelmann, C., Fatigue Performance of Laser Additive Manufactured Ti–6Al–4V in Very High Cycle Fatigue Regime up to 109 Cycles. *Frontiers in Materials*, **2**, article 72, 2015. <https://doi.org/10.3389/fmats.2015.00072>
- [5] Bathias, C., There is no infinite fatigue life in metallic materials. *Fatigue and Fracture of Engineering Materials and Structures*, **22**, pp. 559–566, 1999. <https://doi.org/10.1046/j.1460-2695.1999.00183.x>
- [6] Pyttel, B., Schwerdt, D. & Berger, C., Very high cycle fatigue – Is there a fatigue limit? *International Journal of Fatigue*, **33**, pp. 49–58, 2011. <https://doi.org/10.1016/j.ijfatigue.2010.05.009>
- [7] Frederick, J., *Ultrasonic Engineering*, John Wiley & Sons: New York, NY, 1965.
- [8] Lage, Y., Ribeiro, A., Montalvão, D., Reis, L. & Freitas, M., Automation in strain and temperature control on VHCF with an ultrasonic testing facility. *Journal of ASTM International*, ASTM STP 1571, pp. 80–100, 2014. <https://doi.org/10.1520/stp157120130079>
- [9] Costa, P., Vieira, M., Reis, L., Ribeiro, A. & De Freitas, M., New specimen and horn design for combined tension and torsion ultrasonic fatigue testing in the very high cycle fatigue regime. *International Journal of Fatigue*, **103**, pp. 248–257, 2017. <https://doi.org/10.1016/j.ijfatigue.2017.05.022>
- [10] Cláudio, R., Freitas, M., Reis, L., Li, B., Guelho, I., Antunes, V. & Maia, J., In-Plane Biaxial Fatigue Testing Machine Powered by Linear Iron-Core Motors. *Journal of ASTM International*, ASTM STP 1571, 2014. <https://doi.org/10.1520/stp157120130078>
- [11] Montalvão, D., Shengwen, Q. & Freitas, M., A study on the influence of Ni–Ti M-Wire in the flexural fatigue life of endodontic rotary files by using Finite Element Analysis. *Materials Science and Engineering: C*, **40**, pp. 172–179, 2014. <https://doi.org/10.1016/j.msec.2014.03.061>
- [12] Reis, L., Li, B. & De Freitas, M., A multiaxial fatigue approach to Rolling Contact Fatigue in railways. *International Journal of Fatigue*, **67**, pp. 191–202, 2014, <https://doi.org/10.1016/j.ijfatigue.2014.02.001>

- [13] Baptista, R., Cláudio, R. A., Reis, L., Guelho, I., Freitas, M. & Madeira, J.F.A., Design optimization of cruciform specimens for biaxial fatigue loading. *Frattura ed Integrità Strutturale*, **30**, pp. 118–126, 2014. <https://doi.org/10.3221/igf-esis.30.16>
- [14] Montalvão, D. & Wren, A., Redesigning Axial-Axial (Biaxial) Cruciform Specimens for VHCF Ultrasonic Testing Machines, *Heliyon*, **3(11)**, 2017. <https://doi.org/10.1016/j.heliyon.2017.e00466>
- [15] Costa, P.R., Montalvão, D., Freitas, M., Baxter, R. & Reis, L., Cruciform Specimen's Analysis and Experiments in Ultrasonic Fatigue Testing. *Proceedings of the 18th International Conference on New Trends in Fatigue and Fracture*, Lisbon, Portugal, 2018.
- [16] Bathias, C., Piezoelectric fatigue testing machines and devices. *International Journal of Fatigue*, **28**, pp. 1438–1445, 2006. <https://doi.org/10.1016/j.ijfatigue.2005.09.020>
- [17] Montalvão, D., Freitas, M., Reis, L. & Fonte, M., Design of cruciform test specimens with different biaxiality ratios for VHCF. *Proceedings of the 8th International Conference on Engineering Failure Analysis*, Budapest, Hungary, 2018.
- [18] Blaskovics, A., *Development of Cruciform Specimens for Biaxial VHCF Testing*, BEng Project, Bournemouth University, June 2019 (in progress).
- [19] Silva, J.M.M. & Maia N.M.M. (eds), *Theoretical and Experimental Modal Analysis*, Research Studies Press: Taunton, 1997.